Hadal water biogeochemistry over the Izu-Ogasawara Trench observed with a full-depth CTD-CMS

Shinsuke Kawagucci[1][2][3][#][*], Akiko Makabe[2][3][#], Taketoshi Kodama[4], Yohei Matsui[2][3], Chisato Yoshikawa[2][5], Etsuro Ono[6][$], Masahide Wakita[7], Takuro Nunoura[3][8], Hiroshi Uchida[6], Taichi Yokokawa[3][8][*]

[1]Department of Subsurface Geobiological Analysis and Research (D-SUGAR), Japan Agency for Marine-Earth Science and Technology (JAMSTEC), 2-15 Natsushima-cho, Yokosuka 237-0061, Japan.
[2]Research and Development Center for Submarine Resources (SRRP), Japan Agency for Marine-Earth Science and Technology (JAMSTEC), 2-15 Natsushima-cho, Yokosuka 237-0061, Japan.
[3]Project Team for Development of New-Generation Research Protocol for submarine resources, Japan Agency for Marine-Earth Science and Technology (JAMSTEC), 2-15 Natsushima-cho, Yokosuka 237-0061, Japan.
[4]Japan Sea National Fisheries Research Institute, Japan Fisheries Research and Education Agency, Niigata, Japan, 5939-22 Suido-cho, Niigata 951-8121, Japan.
[5]Department of Biogeochemistry, Japan Agency for Marine-Earth Science and Technology (JAMSTEC), 2-15 Natsushima-cho, Yokosuka 237-0061, Japan.
[6]Research and Development Center for Global Change (RCGC), Japan Agency for Marine-Earth Science and Technology (JAMSTEC), 2-15 Natsushima-cho, Yokosuka 237-0061, Japan.
[7]Mutsu Institute for Oceanography, Japan Agency for Marine-Earth Science and Technology (JAMSTEC), 690 Kitasekine, Mutsu 035-0022, Japan
[8]Research and Development Center for Marine Biosciences, Japan Agency for Marine-Earth Science and Technology (JAMSTEC), 2-15 Natsushima-cho, Yokosuka 237-0061, Japan.
[$]Present address: Japan Meteorological Agency, 1-3-4 Otemachi, Tokyo 100-8122, Japan.
[#]Equally contributed.

Correspondence to: Shinsuke Kawagucci (kawagucci@jamstec.go.jp)
& Taichi Yokokawa (taichi.yokokawa@jamstec.go.jp)

Abstract. Full-depth profiles of hydrographic and geochemical properties at the Izu-Ogasawara Trench were observed for the first time using a CTD-CMS (Conductivity Temperature Depth profiler with Carousel Multiple Sampling) system. Additionally, comparative samplings were done at the northern Mariana Trench using the same methods. A well-mixed hydrographic structure below 7,000 m was observed within the Izu-Ogasawara Trench. Seawater samples collected from this well-mixed hadal layer exhibited constant concentrations of nitrate, phosphate, silicate, and nitrous oxide as well as constant nitrogen and oxygen isotopic compositions of nitrate and nitrous oxide. These results agree well with previous observations of the Izu-Ogasawara hadal waters and deep-sea water surrounding the Izu-Ogasawara Trench. In turn, methane concentrations and isotopic compositions indicated spatial heterogeneity within the well-mixed hadal water mass, strongly suggesting a local methane source within the trench, in addition to the background methane originating from the general

deep-sea bottom water. Sedimentary compound releases, associated with sediment re-suspensions, are considered to be the most likely mechanism for generating this significant CH_4 anomaly.

1 Introduction

5 The CTD-CMS (Conductivity Temperature Depth profiler with Carousel Multiple Sampling) system has been the most essential and fruitful device in the history of oceanography. Seawater sensing by the CTD draws a continuous profile of the general hydrographic properties, while seawater sampling at multiple selected depths by the CMS allows a variety of subsequent analyses for chemical and biological properties. Cross-ocean observations with the CTD-CMS, in some case led by international programs such as WOCE (Siedler et al., 2001) and GEOTRACES (Cutter, 2013), have yielded datasets of

10 comparable qualities and sufficient horizontal resolution that serve as a basis for us to paint the overall picture of the Earth's ocean. However, one blank gap remains in that picture – the hadal waters (deeper than 7,000 m in this study (see Section 3.1) but usually 6,000 or 6,500 m (Jamieson et al., 2010; Watling et al., 2013)), due to the extreme pressure there and a lack of full-depth CTD-CMS systems.

15 The lack of full-depth CTD-CMS systems greatly limited seawater sampling-based analyses and therefore the analysis and understanding of hadal water column in a way comparable to the CTD-CMS data available for all other parts of the ocean. Nevertheless, a small number of hadal sampling efforts, not using the CTD-CMS, have been carried out over the years. For example, a pioneering work (Mantyla and Reid, 1978) collected a total of four hadal seawater samples from two stations in the southern Mariana Trench (MT) with a specially-designed acoustic release device. Hydrographical properties (salinity,

20 oxygen, and nutrients) of the samples obtained demonstrated that hadal and abyssal waters exhibit identical characteristics.

At a trench axis station AN1 (29°05N - 142°51E, 9,750 m) located in the mid Izu-Ogasawara Trench (IOT), vertical seawater samples were collected during two cruises of R/V *Hakuho-maru* in 1984 and 1994 (Nozaki et al., 1998; Gamo and Shitashima, 2018), by directly attaching standard Niskin bottles to a wire line. The samples were used to determine

25 hydrographic properties and for [222]Rn analyses, while three specially-designed samplers were also used for metals and other radionuclides analyses. The hadal water at AN1 exhibited vertically constant profiles in salinity, dissolved oxygen, nitrate, and phosphate, confirming the characteristics previously observed in the southern MT (Mantyla and Reid, 1978). The renewal time of the trench-filling hadal water was evaluated to be ~5 years from the distribution of radionuclides (Nozaki et al., 1998). Manganese and iron were slightly enriched in the hadal water only and were background level in the overlying

30 abyssal water while significant [222]Rn excess was detected in waters up to ~2,700 m above the trench axis seafloor, suggesting lateral [222]Rn supply from the surrounding trench slope (Gamo and Shitashima, 2018). These hadal water-specific characteristics were consistent with a scenario where the transport of sedimentary component from the trench slope to hadal

depths being frequent, which has indeed been commonly shown by sediment observations at trench axes of Izu-Ogasawara, Mariana, Japan, and Tonga trenches (Nozaki and Ohta, 1993; Glud et al., 2013; Oguri et al., 2013; Wenzhofer et al., 2016) and supported by numerical modeling (Ichino et al., 2015).

5   In addition to the geochemical studies outlined above, ~30 vertical seawater samples, including 7 hadal samples, were collected mainly for biological analyses by the remotely operated vehicle *ABISMO* at the Challenger Deep in the southern MT. Phylogenetic analyses from these samples revealed a hadal water-specific microbial community, named the hadal biosphere, which has been shown to be distinct from the abyssal one (Nunoura et al., 2015). Mechanisms developing the hadal biosphere are considered to be likely associated with the lateral supply of sedimentary organic matter from the trench 10   slope and the subsequent activation of microbial community including ammonia and nitrite oxidizers.

Despite these efforts, the spatial coverage within and among trenches, as well as the comprehensiveness of the (bio)geochemical dataset, is still greatly limited compared to other parts of the ocean. To resolve these problems and to obtain data from hadal depths in a directly comparable quality to the global CTD-CMS observations, the development of a 15   full-depth CTD-CMS system is needed and indeed has long been awaited. Ultimately, a full-depth-rated CTD-CMS system was equipped on the research vessel R/V *Kaimei*, launched in 2015. From 2016, the R/V *Kaimei* CTD-CMS system has been deployed at the IOT and the MT including 5 full-depth vertical sequences at trench axes. Here we report the results of (bio)geochemical analyses for these CTD-CMS collected seawater samples, including a total of 57 samples from hadal depths, mostly in the IOT. Tracers for the lateral supply of sedimentary organic matter (methane, manganese, and total 20   organic carbon) and microbial nitrogen metabolisms (nitrate, ammonium, and nitrous oxide) as well as general oceanographic parameters were analyzed.

2. Settings and Methods

2.1   Study area and equipment

25   Seawater column of the IOT and the MT were investigated during 3 R/V *Kaimei* cruises (KM16-02, KM16-08, and KM17-01) and a R/V *Shinsei-maru* cruise (KS-16-8). Locations of the sampling stations are shown in Table 1 and Figure 1. Although the term "hadal" generally refers to the zone below 6,500 m (Jamieson 2015), in this study we use "hadal" for depths below 7000 m and "abyssal" for depths between 4,000-7,000 m, based on the vertical hydrographic constitution revealed by our observations (see Section 3.1). Seawater sampling was generally conducted at 50-250 m vertical intervals at 30   each station.

R/V *Kaimei* has a 12,000m-long synthetic-fiber coaxial cable for the operation of its full-depth CTD-CMS system, which consists of a CTD sensor (SBE911plus, 11,000 m capable), a Carousel water sampler (SBE32, 11,000 m capable) for 36 Niskin-X bottles, and a dissolved oxygen sensor (RINKO, 7,000 m guaranteed but 10,000 m capable). The CTD thermometer (SBE3plus) was calibrated in situ with a deep ocean standard thermometer (SBE35, 7,000 m capable) to correct
5   a pressure dependency of the CTD thermometer (Uchida et al., 2015). The full dataset of the CTD observations will be deposited on a website and discussed elsewhere (Uchida et al., in prep.). R/V *Shinsei-maru* has an 8,000m-long steel coaxial cable for the operation of its CTD-CMS system (6,500 m capable), consisting of a CTD sensor (SBE911plus), a Carousel water sampler (SBE32), 24 Niskin-X bottles, and a dissolved oxygen sensor (SBE43).

2. 2   Analyses

10   The potential density anomaly (σ_{6K}: pref = 6,000 dbar, potential density minus 1,000 kg/m^3) was calculated from the CTD dataset using the TEOS-10 software, calibrated using practical salinity measured. Dissolved oxygen was also measured on the ship using a modified Winkler's titration method (Dickson, 1996). Automatic photometric titrators (DOT-01X or DOT-15X, Kimoto Electronic Co. Ltd., Osaka, Japan) and automatic burettes (APB-410, APB-510, and/or APB-610, Kyoto Electronic Manufacturing Co. Ltd., Tokyo, Japan) for sodium thiosulfate and potassium iodate were used. A precision
15   estimated from standard deviation of replicate measurements was within 0.2 μmol/kg.

Nitrate+nitrite (hereafter, nitrate), phosphate, and silicate concentrations were determined using AutoAnalyzerII (for nitrate and nitrite, Technicon, Dublin, Ireland) and TrAACS 800 (for silicate and phosphate, Bran+Luebbe, Norderstedt, Germany) in Japan Sea National Fisheries Research Institute (Hydes et al., 2010; Kodama et al., 2015). Nutrient samples were frozen in
20   a deep freezer at -80°C immediately after subsampling on-board and stored below -20°C until measurements were taken. Another set of samples was collected during the KM16-08 cruise just for silicate analysis, which were stored at 4°C in the dark and analyzed within two weeks of sampling. In-house standards, prepared using artificial seawater, were used in combination with commercially available nutrient standard solutions (RMNS, KANSO Technos, Tsukuba, Japan) (Aoyama et al., 2012), but only RMNS were used for the standardization of concentrations. RMNS lots of BD, BZ, and BS were used
25   for samples taken during the cruise KM16-02, while BT, BS, and CB were used for KM16-08, and BY, CA, and CB for KM17-01. Phosphate and silicate data could not be obtained for samples taken during KM17-01 due issues with the instrument. The determination limits of nutrient concentrations, defined as tripled standard deviations of blank values, were <0.1, <0.05, and <1 μmol/kg for nitrate, phosphate and silicate, respectively. Analytical errors in our measurement systems, estimated by repeated analyses (n = 5) using the BV lot of RMNS, were 0.48, 0.04, and 0.21 μmol/kg for nitrate, phosphate,
30   and silicate, respectively, as previously reported in the inter-laboratory comparisons of seawater nutrient concentrations (see Aoyama et al., 2016). Seawater for ammonium analysis was subsampled into a 25 mL polypropylene bottle after triple-rinsed with seawater, and ammonium concentration was measured onboard using a fluorometric (OPA) method (Holmes et

al., 1999). The detection limit and analytical precision of ammonium concentrations were as low as 10 nM and ±5 nM (when concentrations was <100 nM), respectively.

Nitrogen and oxygen isotopic compositions of nitrate (and nitrate+nitrite) were analyzed by the denitrification method (Casciotti et al., 2002; McIlvin and Casciotti 2011) at Japan Agency for Marine-Earth Science and Technology (JAMSTEC). A subsample (~50 mL) of seawater was filtered on-board with a 0.45 μm cellulose acetate membrane filer (ADVANTEC) and stored at -20°C. For surface seawater (<500 m) in which nitrite was detected significantly at the AA analysis, sulfamic acid was injected to sample seawater to eliminate nitrite as NO volatile (Granger and Sigman, 2009) while the samples without the acid injection were also analyzed. The isotopic compositions of nitrate+nitrite (without the acid processing) and nitrate (with the acid processing) are annotated by subscripts of N+N and NO3, respectively. The seawater samples were then injected into a laboratory denitrification culture in 20 mL headspace glass vials. Nitrate (and nitrite) was quantitatively converted to nitrous oxide using the strain *Pseudomonas chlororaphis* (JCM20509 = ATCC13985), a denitrifying bacterium lacking the ability to reduce N_2O. International reference materials (IAEA-N3, USGS-32, and USGS-34 for both $\delta^{15}N_{NO3}$ and $\delta^{18}O_{NO3}$, and USGS-35 for $\delta^{18}O_{NO3}$; Böhlke et al., 2003) and in-house working standard were included within a batch of 120 bottles for a series of analysis. The N_2O produced from each culture was then analyzed using a ThermoFinnigan GasBench+PreCon trace gas concentration system, interfaced to a Delta V Plus isotope-ratio mass spectrometer. The conversion efficiency from nitrate to N_2O, evaluated by comparing with the TrAACS 800 analysis, was above 95% in this study. Analytical precisions were estimated to be within 0.2 ‰ for $\delta^{15}N$ and 0.3 ‰ for $\delta^{18}O$. The isotopic compositions of surface seawaters containing significant nitrite were different between the acid-treated and non-treated samples (Table S1) and should be interpreted with caution (e.g., Casciotti and McIlvin, 2007; Kemeny et al., 2016).

The potential nitrification activity was estimated during the KM16-08, KM17-01, and KS-16-8 cruises by ship-based incubation of seawater with 3 ^{15}N-labeled substrates (ammonium, urea, and glutamine) according to an established method (e.g., Shiozaki et al., 2016). Deep-sea water samples were subsampled into 125 mL pre-combusted glass vials. Each of ^{15}N-ammonium, -urea, and -glutamine (amide group-labeled) were then spiked into the vials to give a final concentration of 50 nM, and the samples were incubated at 4 $^{\circ}$C in the dark for 5-10 days prior to filtration (0.45 μm cellulose acetate membrane filer; ADVANTEC). The nitrogen isotopic ratio of the nitrate+nitrite within the filtrate was measured according to same method as for native nitrate analyses, as described above. For comparative purposes, seawater from shallower than 1,000 m were also examined by a similar method, with incubation being carried out under *in situ* temperatures and for a short duration of ≤12 hours. For the calculation of nitrification activity, it was assumed that the concentrations of ammonium, urea, and glutamine were negligible in the native deep-sea water. The detection limit of nitrification activity, determined based on significant changes in the nitrate isotope ratios (>0.6‰, three times higher than the analytical uncertainty) between ^{15}N-spiked and non-spiked seawaters after the incubation, was estimated to be 0.02 nmol/L/day.

The total organic carbon (TOC) concentration was determined using a total organic carbon analyzer (TOC-L, Shimadzu Co., Kyoto, Japan) following a published analytical method (Wakita et al., 2016), with some minor modifications. To determine the TOC, instead of dissolved organic carbon (Wakita et al., 2016), seawater samples were not filtrated on the ship. The TOC concentrations were calibrated using reference materials (provided by Prof. D. A. Hansell (Miami University)) and determined with a precision of ± 1.0 μM. The radiocarbon content (Δ^{14}C) of the dissolved inorganic carbon (DIC) was measured, following the methods published by Kumamoto et al. (2011), at the Institute of Accelerator Analysis Ltd in Shirakawa, Japan (using a Pelletron 9SDH-2, National Electrostatics Corporation, USA) with a 4‰ analytical error.

Concentrations and isotopic compositions of nitrous oxide (N_2O) and methane (CH_4) were determined according to published methods (Hirota et al., 2010) with some modifications for CH_4 purification (Okumura et al., 2016a). Each seawater sample was introduced into a 120 mL glass vial from the Niskin bottle, sealed with a butyl rubber septum and aluminum cap after the addition of 0.2 mL mercury chloride-saturated solution for poisoning, and stored at 4 $^{\circ}$C until the measurement. N_2O and CH_4 dissolved in the seawater were extracted and purified by purge-and-trap gas chromatography prior to the introduction into a MAT253 isotope-ratio mass spectrometer. Resistors of MAT253 Faraday cups for monitoring m/z of 44, 45, and 46 for CO_2 derived from CH_4 oxidation were set respectively at 3×10^9, 3×10^{11}, and 1×10^{12} Ohms, instead of the generally used 3×10^8, 3×10^{10}, and 1×10^{11} Ohms. This modification improved the detection limit of CH_4 to as low as 0.08 nmol/L, while keeping the comparable analytical precision. Errors for analyses conducted during the present study were estimated from repeated analyses of a sample, and were 10% for N_2O concentration, 0.2‰ for $\delta^{15}N_{N2O}$, 0.5‰ for $\delta^{18}O_{N2O}$, 20% for CH_4 concentration, and 0.3‰ for $\delta^{13}C_{CH4}$.

The manganese concentration was measured at onshore laboratory by the Luminol-H_2O_2 chemiluminescence detection method (Ishibashi et al., 1997). For Mn analysis, 100 mL of seawater was drawn from a Niskin bottle to a plastic bottle. As 0.5 mL of ultrapure nitric acid (Tamapure AA-10, Tama Chemical) was added into the sample without filtration, the concentration reported in this study is total dissolvable fraction (e.g., Gamo and Shitashima, 2018). The samplings were conducted during the KM16-08 and KM17-01 cruises. The Mn concentrations were determined within 5% analytical errors and calibrated by simultaneous analysis of an international standard NASS-5 (given concentration 16.7$\pm$1.04 nM).

To examine the validity of our sampling and analyses, nutrients concentrations of abyssal waters at neighbor stations obtained by the WOCE re-occupation program (Stn. 65-90 on P10 line and Stn. 273-321 on P03-revisit line) are selected (Kawano and Uchida, 2007a, 2007b). Basin-scale Δ^{14}C-DO relation below 4,000 dbar from stations of the WOCE P01 (Kawano et al., 2009) and P03 (Kawano and Uchida, 2007a) in addition to P02 (https://cchdo.ucsd.edu/cruise/318M200406) is also used for interpretation.

All analytical results, full-depth vertical profiles, and the overall summary of hadal water analyses are presented in Supplementary Table S1, Supplementary Figure S1, and Table 2, respectively. As the present study focuses on observations and data from deep waters, properties of the surface water are generally used for validating the observations and only discussed minimally.

3. Results

3.1 Major hydrographic property

Vertical profiles of the potential density anomaly (σ_{6K}) revealed that a dense, well-mixed water mass occupies the deeper parts of the trenches (Figure 2a). The boundary between this well-mixed layer and the abyssal layer above is seen as a

10 change in σ_{6K} three times greater than a standard deviation within the nearly-constant density of the well-mixed layer. This boundary was shallower than 7,000 m in all axis stations (Figure 2a). We therefore redefine "hadal" waters as being deeper than 7,000 m in this study although 6,000 or 6,500 m have been used in general (Jamieson et al., 2010; Watling et al., 2013).

Both potential density and DO of the hadal water at the MT station (54.356 and 172 μmol/kg) were higher than those at the

15 IOT stations (54.350 and 164 μmol/kg) (Figure 2a and 2b). These clear differences in properties between hadal waters in the two trenches are in line with the current knowledge from abyssal water observation as northward bottom current in the western Pacific (Wijffels et al., 1998) and the presence of a geographical barrier between IOT and MT (Ogasawara Plateau, Figure 1). Detailed analyses of the CTDO dataset, in addition to its comparison with past CTD(O) observations (Taira et al., 2005; Taira, 2006; Gamo and Shitashima, 2018), will be presented elsewhere (Uchida et al., in preparation).

3.2 Nitrogen biogeochemistry (nitrate, N₂O, ammonium, and potential nitrification activity)

Vertical profiles of nitrate concentrations agreed well among all stations (Figure 2c). Nitrate concentrations of hadal and abyssal waters at IOT stations were almost constant at 35.20±0.41 μmol/kg (n = 47) and 35.50±0.68 μmol/kg (n = 149), respectively (Table 2). The hadal and abyssal nitrate concentrations at the MT stations were 34.72±0.05 μmol/kg (n = 10)

25 and 35.12±0.38 μmol/kg (n = 16), respectively. The nitrate variations in the hadal waters are smaller than the analytical error (0.48 μmol/kg) while a greater nitrate variation in the IOT abyssal water likely reflects a vertical gradient within abyssal zone. Nitrate concentrations of the abyssal waters presented herein were found to be consistent with those at neighboring stations in WOCE P03 and P10 lines (35.36±0.48 μmol/kg; n = 315), confirming accurate quantification. Furthermore, the hadal water value for the IOT agrees well with those observed at AN1 in 1984 (35.1±0.3 μmol/kg) (Gamo and Shitashima,

30 2018).

The $\delta^{15}N_{N+N}$ and $\delta^{18}O_{N+N}$ values in the IOT (Figure 2d, 2e) were also found to be constant through hadal and abyssal layers at $+5.10\pm0.15$‰ and $+2.22\pm0.11$‰ (n = 25, hadal) and $+5.10\pm0.14$‰ and $+2.32\pm0.20$‰ (n = 28, abyssal), respectively (Figure 2 and Table 2). Isotopic characteristics of the deep seawater at the IOT region was consistent with the hadal water at the north MT (as reported herein), the Challenger Deep (Nunoura et al., 2015), and other published reports of deep seawater from the Pacific (e.g., Casciotti, 2016). This isotopic consistency as well as the concentrations suggests little production/consumption of nitrate+nitrite in the IOT hadal water. For waters obtained above 500 m where nitrate concentrations were low (<20 μmol/kg), the isotopic compositions varied between $+3$‰ and $+11$‰ ($\delta^{15}N_{NO3}$ and $\delta^{15}N_{N+N}$) and $+1$‰ and $+22$‰ ($\delta^{18}O_{NO3}$ and $\delta^{18}O_{N+N}$), respectively (Table S1). The low $\delta^{15}N_{NO3}$ and $\delta^{18}O_{NO3}$ values at the surface imply contribution of nitrogen fixation whereas the high $\delta^{15}N_{NO3}$ and $\delta^{18}O_{NO3}$ values could be caused by denitrification (e.g., Casciotti, 2016).

Identical vertical profiles were seen for both N_2O concentrations and isotopic compositions, throughout all stations (Figure 2f, 2g, 2h). N_2O concentrations, $\delta^{15}N_{N2O}$, and $\delta^{18}O_{N2O}$ in hadal and abyssal waters of the IOT were constant at 17.7 ± 1.3 nM, $+8.8\pm0.2$‰, and $+51.6\pm0.3$‰ (n = 47, hadal) and 18.1 ± 1.0 nM, $+8.9\pm0.2$‰, $+51.8\pm0.4$‰ (n = 99, abyssal), respectively (Figure 2 and Table 2). These characteristics of deep-sea N_2O in the IOT region are consistent with those in the MT (this study) and other stations in the north Pacific such as ALOHA (Popp et al., 2002) and KNOT (Toyoda et al., 2002). In turn, variable concentrations (5-42 nM) and isotopic composition ($+6.2$-$+9.5$‰ and $+44$-$+57$‰ for $\delta^{15}N_{N2O}$ and $\delta^{18}O_{N2O}$, respectively) were seen in N_2O above 4,000 m depth in the IOT region, which were not identical with other deep seawater in the Pacific (Toyoda et al., 2017).

Ammonium concentrations at the IOT were not detectable (<10 nM) for both hadal and abyssal waters, while at the surface it was as high as 30 nM. It is consistent with hadal waters from the Challenger Deep that also had negligible ammonium concentration (Nunoura et al., 2015).

The potential nitrification activity of the hadal and abyssal waters in all samples analyzed for the present study was below the determination limit ($\delta^{15}N$ increase smaller than 0.6‰). Even if the $\delta^{15}N$ increase observed (<0.6‰) was significant, the nitrification activity should be not higher than 0.02 nmol/L/day (Figure 3 and Supplementary Table S2). The nitrification activity of the surface water was up to 5 nmol/L/day and comparable to those reported from other oligotrophic stations such as ALOHA and BATS (1-8 nmol/L/day) (Beman et al., 2011), which serves to confirm the validity of our data. At DO minimum depth (~1,500 m), several incubations exhibited detectable nitrification activity (Figure 3). The low potential of nitrification in the deep-sea water (<0.02 nmol/L/day) and the estimated residence time of hadal water (~5 years: Nozaki et al., 1998) are not inconsistent with the negligible changes in nitrate (~35 μmol/kg) and nitrous oxide (~18 nM,).

3. 3 Phosphate, silicate, radiocarbon, TOC, and manganese

Phosphate concentrations at each station were generally constant through hadal and abyssal depths (Figure 2i). For example, samples from the KM16-08 cruise exhibited phosphate concentrations of 2.40±0.01 μmol/kg for hadal waters (n = 11) and 2.42±0.02 μmol/kg for abyssal waters (n = 21), respectively, demonstrating a lack of hadal-specific phosphate cycle. Hadal phosphate concentrations during the KM16-08 cruise were consistent with those reported for hadal waters at AN1 in 1984 (2.39±0.04 μmol/kg)(Gamo and Shitashima, 2018) and for abyssal water (below 5,500 dbar) at neighboring stations of WOCE P03 and P10 (2.44±0.02 μmol/kg, n = 77). A few systematic differences seemed present in phosphate concentrations among the different cruises (Figure 2i) while the N-P relationships within each cruise were clearly linear (Supplementary Table S1).

Silicate concentrations were highly variable (Figure 2j). However, the variation was probably caused due to freezing and thawing of the samples as discussed previously by Zhang and Ortner (1998). Compared to silicate distributions of the WOCE P03 and P10 lines, samples maintained at 4°C from the KM16-08 cruise showed consistent vertical profiles but the -20°C frozen samples from the other cruises generally showed lower concentrations. At stations sampled during KM16-08 (34N02 and 34N03), silicate concentrations were constant within the hadal water (145.6±0.2 μmol/kg, n = 11) but slightly variable in the abyssal water (148.9±2.3 μmol/kg, n = 21) due to the presence of a vertical gradient. Concentrations measured from samples obtained at KM16-08 stations were consistent with those reported from LM2 (~143 μmol/kg) (Gamo and Shitashima, 2018) but slightly higher than those of the abyssal water (below 5,500 dbar) at neighboring stations of WOCE P03 and P10 (134.7±2.43 μmol/kg, n = 77).

The radiocarbon contents (Δ^{14}C) of the hadal and abyssal waters at the IOT and the MT were constant within each water layer: -206.6±4.4‰ (n = 40, IOT hadal), -209.8±7.4‰ (n = 62, IOT abyssal), -197.0±3.9‰ (n = 10, MT hadal), and -210.0±5.8‰ (n = 16, MT abyssal) (Figure 2k and Table 2). The variation in Δ^{14}C for hadal depths, comparable to the analytical error (±4‰), is reasonable because the change in Δ^{14}C is expected to be <1‰ from the estimated renewal time of ~5 yr (Nozaki et al., 1998) and the Δ^{14}C-yr relationship of 8.7 yr/‰ (Sarmiento and Gruber, 2006). The DO-Δ^{14}C relationships within the hadal water mass ranged within those of the Pacific deep seawater from WOCE P01-P03 (Figure 4). Variations of DO and Δ^{14}C within the hadal water mass were too small for evaluating trench-specific oxygen consumption rates, but the DO-Δ^{14}C relationship of the Pacific deep seawater yields a slope of 0.749±0.030 μmol/kg/‰, corresponding to an oxygen consumption rate of 0.0860±0.0034 μmol/kg/yr.

The concentrations of TOC in the deep seawater (below 2,000 m) of the IOT and MT regions were rather constant at ~38 μM with the exception of a few samples (Figure 2l and Table S2). This TOC level agrees well with DOC observations at a neighboring abyssal plain station (S1: 30°N - 145°E) (http://ebcrpa.jamstec.go.jp/k2s1/en/index.html). The TOC

concentrations at the stations 34N02 and 31N03 appear to be increasing from 8,000 and 9,000 m towards the bottom, respectively, despite the well-mixed hydrographic property. The observed increases are significant beyond the analytical uncertainty of ±1 μM (Figure 2l). The hadal TOC gradient strongly suggests inner-trench TOC input since negligible TOC catabolism is expected from the negligible DO change (<0.1 μmol-O_2/kg). Abyssal samples collected at 32N during the KS-16-8 cruise also exhibited TOC concentrations higher than 40 μM.

Manganese concentrations of the hadal and abyssal waters at the IOT (except the 34N03 samples) and the MT were 0.71±0.27 nM (n = 35, IOT hadal), 0.33±0.21 nM (n = 39, IOT abyssal), 0.04±0.04 nM (n = 10, MT hadal), and 0.19±0.09 nM (n = 16, MT abyssal) (Figure 2m). While the abyssal Mn concentrations were comparable between the IOT and MT, the hadal Mn concentrations were significantly higher at the IOT. Vertically, the Mn concentrations at the IOT and MT seemed higher and lower at the hadal depth, respectively. The hadal Mn ranges at the IOT were comparable between this study (0.3 - 1.6 nM) and previous study (0.6 - 1.4 nM)(Gamo and Shitashima, 2018). The abyssal water at 34N03 showed Mn increase toward the seafloor while anomalously high background level of ~0.5 nM only at 34N03 implies a possibility of contamination during the CTD-CMS sampling.

3. 4   Methane

Methane concentrations were generally as low as 0.25 nM below 2,000 m deep (Figure 2n). CH_4 concentrations as low as 0.25 nM are ubiquitous in deep-sea water (Hirota et al., 2010; Son et al., 2014) and probably regulated by a minimum threshold in microbial uptake for aerobic methanotrophy. Opposite to the general trend, an increase of methane concentrations to three times higher than the general level was detected in waters below 8,000 m deep at the station 34N02 (Figure 2n), despite well-mixed hydrographic property.

$\delta^{13}C$ values of CH_4 were highly variable between -60‰ and -30‰ (Figure 2o), despite there being little variation in concentrations among the sites (Figure 2n). A clear spatial trend in $\delta^{13}C_{CH4}$ values was observed in the IOT region (Figure 5). Vertically, $\delta^{13}C_{CH4}$ values were ~-38‰ between 4,000-6,000 m and then generally decreased with increasing depth, and became constant below 8,000 m (Figure 2o). Below 8,000m, $\delta^{13}C_{CH4}$ values exhibited a north-south trend where the values were lower (-56.2±1.4‰: n = 7) at 34N than the other IOT stations (-46.3±2.2‰: n=23) and also the MT stations (-35.5±3.7‰: n = 5)(Figures 2o and 5). Moreover, values measured from abyssal waters suggested a west-east trend, with $\delta^{13}C_{CH4}$ from the western stations (relative to the axis: Figure 1) being generally lower than -40‰ and from the eastern stations generally higher than -40‰ (Figure 5).

4. Discussion

4.1 Sedimentary compound release through sediment re-suspension at slopes

The CH_4 heterogeneity, despite the well-mixed hydrographic properties, in the IOT hadal water strongly suggests the occurrence of local CH_4 source(s) within the trench, in addition to the deep Pacific seawater-sourced background CH_4. The

5   background CH_4 has a concentration of ~0.25 nM with $\delta^{13}C_{CH4}$ of -38‰, while the CH_4 from the local source would have $\delta^{13}C_{CH4}$ of ~-58‰, as observed in the 34N hadal water. The moderate $\delta^{13}C_{CH4}$ value observed in the hadal waters from 27-32N can be attributed to the kinetic isotope effect of microbial methane consumption, which causes ^{13}C enrichment in the remnant CH_4 (Tsunogai et al., 2000; Feisthhuer et al., 2011), in addition to water mass mixing (Figure 6). Assuming the endmember composition of the local CH_4 source within the trench being 1.0 nM with $\delta^{13}C_{CH4}$ of -58‰ and taking the

10   probable range of kinetic isotope effects (ε = 5‰ - 20‰) (Tsunogai et al., 2000; Feisthhuer et al., 2011) into consideration, the compositional and isotopic variation of CH_4 observed in the IOT can be reasonably explained (Figure 6). The microbial consumption of CH_4 in sub-nano-molar quantities, if it occurs, is not in conflict with the negligible change in DO observed, the detection limit of which is ~100 nmol/kg. It is also the case for the negligible change in $\Delta^{14}C$ because the DIC concentration (~2.3 mM) was 6-7 orders of magnitude higher than CH_4 concentration. Multiple CH_4 local sources with

15   different ^{13}C signatures, other than the 34N source proposed above, are also a possibility in generating the $\delta^{13}C_{CH4}$ variations observed within the IOT hadal water, and does not conflict with the discussion above.

The observed ^{13}C-depleted CH_4 at the northern and western stations appears to be consistent with known two bottom water currents. In addition to a generally northward-flowing basin-scale bottom current, a local counter-clockwise current at

20   ~6,000 m deep in the IOT was revealed by previous current meters deployment on the seafloor at 34N (Fujio et al., 2000). The basin-scale current brings the background CH_4 into the eastern sill of the IOT. On the other hand, the local counter-clockwise current, particularly southward current along with western slope, distributes the ^{13}C-depleted CH_4-rich water occurring at 34N to the western part of inner trench water, resulting in $\delta^{13}C_{CH4}$ values being lower on the western side on the 31N line. Also, the north-south trend in $\delta^{13}C_{CH4}$ below 8,000 m mentioned above can be explained by a north-south mixing

25   between the local ^{13}C-depleted CH_4 at 34N and the background CH_4 from the Ogasawara Plateau region. Nevertheless, multiple CH_4 sources in addition to the proposed 34N source can also generate the observed spatial heterogeneity in $\delta^{13}C_{CH4}$ values.

Several local CH_4 sources are known in the deep-sea, but it appears very unlikely for most of them to be accountable for the

30   hadal CH_4 and other geochemical anomalies seen in the IOT, such as TOC, Mn, and ^{222}Rn (Gamo and Shitashima, 2018). Firstly, the discharge of high-temperature hydrothermal fluid is a well-known source for deep-sea CH_4 plumes that are accompanied with Mn, Fe, and ^{222}Rn (e.g., Kadko et al. 1990; Resing et al. 2015). However, hydrothermal vents in the Izu-Ogasawara region are only expected to occur at the volcanic arc and back arc with depths of ~1,500 m (e.g. Tsunogai et al.

1994). Secondly, cold fluid seepage at accretionary prisms contains abundant CH_4 (e.g., Toki et al. 2004), but is unlikely to occur at the IOT which is non-accretionary. Thirdly, serpentinization-associated CH_4-rich geofluids have been reported from seafloors where (sea)water penetrates into peridotite (Fryer 2011; Kelley et al. 2005). An example has been reported from the terrestrial-ward slope of the Challenger Deep, southern MT (Okumura et al., 2016b). The exposure of serpentinized peridotite below 5,500 m at the terrestrial-ward slope of the IOT (Morishita et al., 2011; Harigane et al., 2013) indicates that discharge of CH_4-rich geofluids occurring in the IOT cannot be ruled out, but such geofluid systems have never been discovered before. Seafloor serpentinization geofluids reported so far exhibit $\delta^{13}C_{CH4}$ values higher than -40‰ (Konn et al., 2015) and are not compatible with the hadal CH_4 anomaly observed in this study. Also, it appears unlikely for highly alkaline serpentinization-based geofluids to generate Mn and Fe plumes. In addition to the fluid releases, *in situ* microbial methanogenesis in deep-sea water column, which could generate ^{13}C-depleted CH_4 if it does occur (e.g., Okumura et al., 2016a), is also very unlikely due to high DO levels through the water column in the IOT (e.g., Reeburgh, 2007).

Sedimentary compounds released into the water column, through sediment re-suspension, is therefore the most likely process responsible for generating the CH_4 (and TOC) anomaly in the IOT water mass, as previously proposed for other hadal-specific geochemical anomalies in Mn and ^{222}Rn (Gamo and Shitashima, 2018) and microbiological characteristics (Nunoura et al., 2015). Earthquake-induced sediment re-suspension and the associated increase in turbidity as well as anomalies in CH_4 and Mn have been occasionally reported in the deep-sea water column (Tsunogai et al., 1996; Gamo et al., 2007; Kawagucci et al., 2012). Values of $\delta^{13}C_{CH4}$ ranging from -80‰ to -60‰ were observed in the turbid seawater (Kawagucci et al., 2012) and the shallow part of seafloor sediment (Ijiri et al., 2008; Heuer et al., 2009), compatible to that of the hadal water at the 34N stations. The CH_4 released is attributable to both CH_4 dissolved in porewater and CH_4 adsorbed on sediment surface although they cannot be distinguished by water column observation. Also, the increase in TOC observed is attributable to both suspended organic particles directly entrained into the Niskin bottles and the dissolved organic matter stripped from the suspended particles (Komada and Reimers, 2001). Alternatively, the little changes in $\delta^{13}C_{CH4}$, Mn, and TOC through hadal and abyssal waters at the 24N stations suggest little input of sedimentary compound at the north end of MT.

Explanation for a vertical layer ~2,000 m in thickness exhibiting anomalously high CH_4 (this study) and ^{222}Rn (Gamo and Shitashima, 2018) requires sedimentary compounds to be released not only from the axis bottom, but also from the trench slopes. Re-suspensions from the trench slope have been commonly suggested by sediment observations that identified rapid accumulation of the axis sediment, in association with frequent sediment transports from slopes (Nozaki and Ohta, 1993; Glud et al., 2013; Oguri et al., 2013; Luo et al., 2018). As earthquake-induced turbid seawater was indeed evident over the trench slope after earthquake events (Gamo et al., 2007; Kawagucci et al., 2012), this geological force is probably an episodic driver for re-suspension in the IOT. On the other hand, oceanographic forces, such as tidal oscillations and eddy diffusions associated with bottom currents, are weaker but more ubiquitously occurring drivers of re-suspension in the overall deep-sea environment including the hadal trench. Intense nepheloid bottom layers over the abyssal plain, also

generated by sediment re-suspension, have been found in regions where bottom current regimes are both strong and variable (e.g. de Madron et al., 2017). The strong bottom current at the IOT sills (Fujio et al., 2000) combined with complex seafloor topography of the trench walls (Figure 1), therefore, likely facilitates re-suspension in the IOT. Nevertheless, the spatio-temporal distribution of the sediment re-suspension events within a trench, magnitudes and durations of the relevant geochemical anomalies in hadal and abyssal waters, and mechanisms driving such re-suspensions, remain poorly understood overall.

4.2 Energetics of the hadal biosphere

The microbial community inhabiting hadal waters has been shown to be distinct from the abyssal counterpart (Nunoura et al., 2015). For the formation of the hadal biosphere, a certain amount of energy is necessarily required. The minimum energy required to shift one microbial community to another without cell density change should be not lower than the energy to maintain cell density of the microbial community. The cell-specific energy requirement for 'maintenance', when cells only carry out basic metabolic functions and activities without new growth, has been suggested to be 10^{-18} kJ/cell/sec (= 3×10^{-11} kJ/cell/yr) (Hoehler, 2004). On the other hand, the potential energy yield of the IOT hadal-abyssal water through ammonium oxidation can be calculated from the maximum rate estimated in the present study (<0.02 nmol-N/L/day (= <7.3 nmol-N/L/yr)) and the Gibbs free energy of aerobic oxidation of ammonium to nitrate (305 kJ/mol-N), to be $<2.2\times10^{-6}$ kJ/L/yr. Evaluation of the energy potentials for maintenance (3×10^{-11} kJ/cell/yr) and yield ($<2.2\times10^{-6}$ kJ/L/yr) indicates that the ammonium oxidation in the hadal-abyssal water column can maintain $<10^{5}$ cell/L. Since cell densities in the hadal-abyssal water column are typically in the order of 10^{6} cell/L (e.g., Nunoura et al., 2015), this energetic calculation suggests that, in terms of energy flux, the ammonium oxidation would only occupy a minor role in characterizing the hadal ecosystem. In turn, the oxygen consumption rate in deep Pacific seawater (0.086±0.003 μmol-O_2/kg/yr), evaluated from the Δ^{14}C-DO relationship (see Section 3.4), is approximately an order of magnitude higher than the maximum rate possible for the ammonium oxidation-specific oxygen consumption (<0.018 μmol-O_2/kg/yr). If the DO-normalized potential energy yields are the same between aerobic catabolism of deep-sea TOC and ammonium oxidation, the TOC catabolism yields 1.4×10^{-5} kJ/kg/yr. This potential energy yield provides a reasonable explanation for the density of microbes observed in the deep-sea water column (~10^{6} cell/L). Although this yield may be insufficient for explaining the rapid turnover of microbial community from the abyssal water community into the hadal biosphere, we are aware that the accurate evaluation of the actual yield requires some more factors to be determined for the hadal water. For an example, the *in situ* oxygen consumption rate in the IOT hadal-abyssal water is assumed to be the same as Pacific deep-sea-averaged level in the above calculation. For another example, the potential energy yield of TOC catabolism is assumed to be the same as ammonium oxidation in the above calculation. In particular, the oxygen consumption rate is likely higher in the IOT hadal water than the deep Pacific seawater used in the calculation above, because sediment re-suspension introduces more labile sedimentary

organic compound (Nunoura et al., 2013; Wenzhöfer et al., 2016) in addition to the background TOC. The same also applies to the maintenance energy used, which has not been strictly constrained (Hoehler 2004).

5. Conclusion

Using full-depth CTD-CMS observation and sampling, the present study revealed heterogeneous distributions of CH_4 within the well-mixed hadal water. We interpret that sediment re-suspension, accompanied by the release of sedimentary compounds into the water column, is the most likely source for the CH_4 anomaly as well as other geochemical anomalies in the hadal layer reported in previous studies and also observed in the present study. From an energetics viewpoint, microbial ammonium oxidation was shown to only occupy a minor part for the overall microbial oxygen consumption expected in the hadal water column. A great advantage with using the CTD-CMS system to study hadal waters, compared to unconventional methods used in previous studies, is the amount of water that can be sampled using a Carousel sampler. The biogeochemical analyses undertaken in this study only used a ~2L subsample out of 12L seawater sample collected by each Niskin bottle, and the remaining are available for further analyses such as microbiological characterization. To shed the fullest light on the dark hadal biosphere, comprehensive analyses combining hydrography, (bio)geochemistry, and microbiology is indispensable, and full-depth CTD-CMS systems (such as the one available on R/V *Kaimei*) put such studies within our reach.

Data availability

Dataset reported is available in Table S1 and on-line at http://www.jamstec.go.jp/iorgc/ocorp/data/kate/.

Supplement file

Supplement Table S1: All analytical results drawn in figures.

Supplement Table S2: Raw data of nitrification activity measurement.

Supplement Figure S1: Full-depth profiles.

Author contribution

SK, TN, HU, and TY designed the study. AM, TK, YM, CY, EO, MW, and HU conducted chemical and hydrographic analyses. SK, AM, and TY made a draft. All authors contributed to sampling and gave final approval for submission and publication.

Competing interest

The authors declare that they have no conflict of interest.

Acknowledgement

The authors thank Katsuhisa Maeno, Yosaku Maeda, the masters, crews, and scientific parties including MWJ and NME staffs of R/V Kaimei cruises (KM16-02, KM16-08, and KM17-01) and a R/V Shinsei-maru cruise (KS-16-8) for their

5   support. Keiko Tanaka, Shoko Tatamisashi, and Dr. Yuichiro Kumamoto respectively supported the CH_4, TOC, and radiocarbon analyses. Dr Chong Chen kindly made English editing. Dr Konomi Suda, Dr Yuya Tada, Dr Michinari Sunamura, Miho Hirai, and Yoko Sasaki helped subsampling on board. Dr Kazuya Kitada analyzed and drew seafloor topography. Manganese analyses were supported by Kaiyo Keisoku Co. Ltd. (president: Dr. Kei Okamura).

10   **References**

Aoyama, M., Ota, H., Kimura, M., Kitao, T., Mitsuda, H., Murata, A. and Sato, K.: Current Status of Homogeneity and Stability of the Reference Materials for Nutrients in Seawater. Analytical Sciences, 28, 911-916, 2012.

Aoyama, M., Abad, M., Anstey, C., Ashraf P, M., Bakir, A., Becker, S., Bell, S., Berdalet, E., Blum, M., Briggs, R., Caradec, F., Cariou, T., Church, M., Coppola, L., Crump, M., Curless, S., Dai, M., Daniel, A., Davis, C. E., De Santis Braga, E.,

15   Solis, M. E., Ekern, L., Faber, D., Fraser, T., Gundersen, K., Jacobsen, S., Knockaert, M., Komada, T., Kralj, M., Kramer, R., Kress, N., Lainela, S., Ledesma, J., Li, X., Lim, J.-H., Lohmann, M., Lonborg, C., Ludwichowski, K.-U., Mahaffey, C., Malien, F., Margiotta, F., Mccormack, T., Murillo, I., Naik, H., Nausch, G., Olafsdottir, S. R., Van Ooijen, J., Paranhos, R., Payne, C., Pierre-Duplessix, O., Prove, G., Rabiller, E., Raimbault, P., Reed, L., Rees, C., Rho, T., Roman, R., Woodward, E. M. S., Sun, J., Szymczycha, B., Takatani, S., Taylor, A., Thamer, P., Torres-Valdes, S., Trahanovsky,

20   K., Waldron, H., Walsham, P., Wang, L., Wang, T., White, L., Yoshimura, T. and Zhang, J.-Z. (Eds.): IOCCP-JAMSTEC 2015 Inter-laboratory Calibration Exercise of a Certified Reference Material for Nutrients in Seawater, JAMSTEC, Yokosuka, Japan, 2016.

Beman, J. M., Cheryl-Emiliane, C., King, A. L., Feng, Y., Fuhrman, J. A., Andersson, A., Bates, N. R., Popp, B. N. and Hutchins, D. A.: Global declines in oceanic nitrification rates as a consequence of ocean acidification, Proceedings of the

25   National Academy of Sciences of the United States of America, 108, 208–213, doi:10.1073/pnas.1011053108, 2011.

Böhlke, J. K., Mroczkowski, S. J. and Coplen, T. B.: Oxygen isotopes in nitrate: new reference materials for ^{18}O: ^{17}O: ^{16}O measurements and observations on nitrate-water equilibration, Rapid Communications in Mass Spectrometry, 17(16), 1835–1846, doi:10.1080/10256019808234072, 2003.

Casciotti, K. L.: Nitrogen and Oxygen Isotopic Studies of the Marine Nitrogen Cycle, Annu. Rev. Mar. Sci., 8(1), 379–407,

30   doi:10.1146/annurev-marine-010213-135052, 2016.

Casciotti, K.L. and McIlvin, M.R.: Isotopic analyses of nitrate and nitrite from reference mixtures and application to Eastern Tropical North Pacific waters, Marine Chemistry, 107, 184-201, 2007.

Casciotti, K. L., Sigman, D. M., Galanter Hastings, M., Böhlke, J. K. and Hilkert, A.: Measurement of the Oxygen Isotopic Composition of Nitrate in Seawater and Freshwater Using the Denitrifier Method, Anal. Chem., 74, 4905–4912, doi:10.1021/ac020113w, 2002.

Cutter, G. A.: Intercalibration in chemical oceanography-Getting the right number, Limnology and Oceanography: Methods, 11, 418–424, doi:10.4319/lom.2013.11.418, 2013.

de Madron, D. X., Ramondenc, S., Berline, L., Houpert, L., Bosse, A., Martini, S., Guidi, L., Conan, P., Curtil, C., Delsaut, N., Kunesch, S., Ghiglione, J. F., Marsaleix, P., Pujo-Pay, M., Séverin, T., Testor, P., Tamburini, C.the ANTARES collaboration: Deep sediment resuspension and thick nepheloid layer generation by open-ocean convection, J. Geophys. Res. Oceans, 122(3), 2291–2318, doi:10.1016/j.margeo.2006.10.034, 2017.

Dickson, A.: Determination of dissolved oxygen in sea water by Winkler titration, WOCE Operations Manual, WHPO 91-1, rev. 1, November 1994, Woods Hole Mass., USA, 1996.

Feisthauer, S., Vogt, C., Modrzynski, J., Szlenkier, M., Krüger, M., Siegert, M. and Richnow, H.-H.: Different types of methane monooxygenases produce similar carbon and hydrogen isotope fractionation patterns during methane oxidation, Geochimica et Cosmochimica Acta, 75(5), 1173–1184, doi:10.1016/j.gca.2010.12.006, 2011.

Fryer, P.: Serpentinite Mud Volcanism: Observations, Processes, and Implications, Annu. Rev. Mar. Sci., 4(1), 345–373, doi:10.1146/annurev-marine-120710-100922, 2012.

Fujio, S., Yanagimoto, D. and Taira, K.: Deep current structure above the Izu-Ogasawara Trench, J. Geophys. Res., 105(C3), 6377–6386, 2000.

Gamo, T. and Shitashima, K.: Chemical characteristics of hadal waters in the Izu-Ogasawara Trench of the western Pacific Ocean, Proc. Jpn. Acad., Ser. B, 94, 45–55, doi:10.2183/pjab.94.004, 2018.

Gamo, T., Okamura, K., Mitsuzawa, K. and Asakawa, K.: Tectonic pumping: earthquake-induced chemical flux detected in situ by a submarine cable experiment in Sagami Bay, Japan, Proc. Jpn. Acad., Ser. B, 83, 199–204, doi:10.2183/pjab/83.199, 2007.

Glud, R. N., Wenzhöfer, F., Middelboe, M., Oguri, K., Turnewitsch, R., Canfield, D. E. and Kitazato, H.: High rates of microbial carbon turnover in sediments in the deepest oceanic trench on Earth, Nature Geoscience, 6(4), 284–288, doi:10.1038/ngeo1773, 2013.

Granger, J. and Sigman, D.M.: Removal of nitrite with sulfamic acid for nitrate N and O isotope analysis with the denitrifier method, Rapid Commun. Mass Spectrom., 23, 3753-3762, 2009.

Harigane, Y., Michibayashi, K., Morishita, T., Tani, K., Dick, H. J. B. and Ishizuka, O.: The earliest mantle fabrics formed during subduction zone infancy, Earth and Planetary Science Letters, 377, 106-113, doi:10.1016/j.epsl.2013.06.031, 2013.

Heuer, V. B., Pohlman, J. W., Torres, M. E., Elvert, M. and Hinrichs, K.-U.: The stable carbon isotope biogeochemistry of acetateand other dissolved carbon species in deep subseafloor sediments at the northern Cascadia Margin, Geochimica et Cosmochimica Acta, 73(11), 3323–3336, doi:10.1016/j.gca.2009.03.001, 2009.

Hirota, A., Tsunogai, U., Komatsu, D. D. and Nakagawa, F.: Simultaneous determination of $\delta^{15}N$ and $\delta^{18}O$ of N_2O and $\delta^{13}C$ of CH_4 in nanomolar quantities from a single water sample, Rapid Communications in Mass Spectrometry, 24, 1085–1092, doi:10.1002/rcm.4483, 2010.

Hoehler, T. M.: Biological energy requirements as quantitative boundary conditions for life in the subsurface, Geobiology, 2, 205–215, 2004.

Holmes, R. M., Aminot, A., Kerouel, R., Hooker, B. A. and Peterson, B. J.: A simple and precise method for measuring ammonium in marine and freshwater ecosystems, Canadian Journal of Fisheries and Aquatic Sciences, 56, 1801–1808, 1999.

Hydes, D., Aoyama, M., Aminot, A., Bakker, K., Becker, S., Coverly, S., Daniel, A., Dickson, A., Grosso, O., Kerouel, R., Van Ooijen, J., Sato, K., Tanhua, T., Woodward, M., Zhang, J.: Determination of dissolved nutrients (N, P, Si) in seawater with high precision and inter-comparability using gas-segmented continuous flow analysers, in: The GO-SHIP Repeat Hydrography Manual: A Collection of Expert Reports and guidelines Version 1, IOCCP Report 14, ICPO Publication Series 134, 2010. (available on-line at http://archimer.ifremer.fr/doc/00020/13141/)

Ichino, M. C., Clark, M. R., Drazen, J. C., Jamieson, A., Jones, D. O. B., Martin, A. P., Rowden, A. A., Shank, T. M., Yancey, P. H. and Ruhl, H. A.: Deep-Sea Research Part I, 100(C), 21–33, doi:10.1016/j.dsr.2015.01.010, 2015.

Ijiri, A., Tsunogai, U., Gamo, T., Nakagawa, F., Sakamoto, T. and Saito, S.: Enrichment of adsorbed methane in authigenic carbonate concretions of the Japan Trench, Geo-Mar Lett, 29(5), 301–308, doi:10.1016/0146-6380(90)90068-B, 2009.

Ishibashi, J., Wakita, H., Okamura, K., Nakayama, E., Feely, R.A., Lebon, G.T., Baker, E.T., Marumo, K.: Hydrothermal methane and manganese variation in the plume over the superfast-spreading southern East Pacific Rise, Geochimica et Cosmochimica Acta, 61(3), 485-500, 1997.

Jamieson, A. (Ed.): The Hadal Zone – Life in the Deepest Ocean. Cambridge University Press, Cambridge, UK, 2015.

Jamieson, A., Fujii, T., Mayor, D.J., Solan, M., Priede, I.G.: Hadal trenches: the ecology of the deepest places on Earth, Trends in Ecology and Evolution, 25, 190-197, 2010.

Kadko, D. C., Rosenberg, N. D., Lupton, J. E., Collier, R. W. and Lilley, M. D.: Chemical reaction rates and entrainment within the Endeavour Ridge hydrothermal plume, Earth and Planetary Science Letters, 99, 315–335, 1990.

Kawagucci, S., Yoshida, Y. T., Noguchi, T., Honda, M. C., Uchida, H., Ishibashi, H., Nakagawa, F., Tsunogai, U., Okamura, K., Takaki, Y., Nunoura, T., Miyazaki, J., Hirai, M., Lin, W., Kitazato, H. and Takai, K.: Disturbance of deep-sea environments induced by the M9.0 Tohoku Earthquake, Sci Rep, 2(1), 1135, doi:10.1111/j.1574-6941.2008.00636.x, 2012.

Kawano, T. and Uchida, H. (eds.): WHP P03 Revisit Data Book, JAMSTEC, Yokosuka, Japan, 2007a. (available on-line at http://www.jamstec.go.jp/iorgc/ocorp/data/p03rev_2005/)

Kawano, T. and Uchida, H. (eds.): WHP P10 Revisit Data Book, JAMSTEC, Yokosuka, Japan, 2007b. (available on-line at http://www.jamstec.go.jp/iorgc/ocorp/data/p10rev_2005/)

Kawano, T., Uchida, H. and Doi, T. (eds.): WHP P01, P14 Revisit Data Book, JAMSTEC, Yokosuka, Japan, 2009. (available on-line at http://www.jamstec.go.jp/iorgc/ocorp/data/p01_p14rev_2007/)

Kelley, D. S., Karson, J. A., Früh-Green, G. L., Yoerger, D. R., Shank, T. M., Butterfield, D. A., Hayes, J. M., Schrenk, M. O., Olson, E. J., Proskurowski, G., Jakuba, M., Bradley, A., Larson, B., Ludwig, K., Glickson, D., Buckman, K., Bradley, A. S., Brazelton, W. J., Roe, K., Elend, M. J., Delacour, A., Bernasconi, S. M., Lilley, M. D., Baross, J. A., Summons, R. E. and Sylva, S. P.: A Serpentinite-Hosted Ecosystem: The Lost City Hydrothermal Field, Science, 307, 1428–1434, 2005.

Kemeny, P.C., Weigand, M.A., Zhang, R., Carter, B.R., Karsh, K.L., Fawcett, S.E. and Sigman, D.M.: Enzyme-level interconversion of nitrate and nitrite in the fall mixed layer of the Antarctic Ocean, Global Biogeochemical Cycles, 30, 1069-1085, doi:10.1002/ 2015GB005350, 2016.

Kodama, T., Morimoto, H., Igeta, Y. and Ichikawa, T.: Macroscale-wide nutrient inversions in the subsurface layer of Japan Sea during summer. J. Geophys. Res. 120: 7476-7492, 2015.

Konn, C., Charlou, J. L., Holm, N. G. and Mousis, O.: The Production of Methane, Hydrogen, and Organic Compounds in Ultramafic-Hosted Hydrothermal Vents of the Mid-Atlantic Ridge, Astrobiology, 15(5), 381–399, doi:10.1089/ast.2014.1198, 2015.

Komada, T. and Reimers, C. E.: Resuspension-induced partitioning of organic carbon between solid and solution phases from a river–ocean transition, Marine Chemistry, 76, 155–174, 2001.

Kumamoto, Y., Murata, A., Kawano, T., Watanabe, S. and Fukasawa, M.: Decadal changes in bomb-produced radiocarbon in the Pacific ocean from the 1990s to 2000s, Radiocarbon, 55, 1641–1650, 2013.

Luo, M., Glud, N.R., Pan, B., Wenzhöfer, F., Xu, Y., Lin, G., Chen, D.: Benthic carbon mineralization in hadal trenches: Insights from in-situ determination of benthic oxygen consumption, Geophysical Research Letters, 45, 2752-2760, 2018.

Mantyla, A. W. and Reid, J. L.: Measurements of water characteristics at depths greater than 10km in the Marianas Trench, Deep-Sea Research, 25, 169–173, 1978.

Morishita, T., Tani, K., Shukuno, H., Harigane, Y., Tamura, A., Kumagai, H. and Hellebrand, E.: Diversity of melt conduits in the Izu-Bonin-Mariana forearc mantle: Implications for the earliest stage of arc magmatism, Geology, 39(4), 411–414, doi:10.1130/G31706.1, 2011.

Nozaki, Y. and Ohta, Y.: Rapid and frequent turbidite accumulation in the bottom of Izu-Ogasawara Trench: Chemical and radiochemical evidence, Earth and Planetary Science Letters, 120, 345–360, 1993.

Nozaki, Y., Yamada, M., Takashi, N., Yutaka, N., Nakamura, K., Shitashima, K. and Tsubota, H.: The distribution of radionuclides and some trace metals in the water columns of the Japan and Bonin trenches, Oceanologica Acta, 21(3), 469–484, 1993.

Nunoura, T., Nishizawa, M., Kikuchi, T., Tsubouchi, T., Hirai, M., Koide, O., Miyazaki, J., Hirayama, H., Koba, K. and Takai, K.: Molecular biological and isotopic biogeochemical prognoses of the nitrification-driven dynamic microbial nitrogen cycle in hadopelagic sediments, Environ Microbiol, 15(11), 3087–3107, doi:10.1111/1462-2920.12152, 2013.

Nunoura, T., Takaki, Y., Hirai, M., Shimamura, S., Makabe, A., Koide, O., Kikuchi, T., Miyazaki, J., Koba, K., Yoshida, N., Michinari, S. and Takai, K.: Hadal biosphere: Insight into the microbial ecosystem in the deepest ocean on Earth, Proceedings of the National Academy of Sciences of the United States of America, 112 (11), E1230–E1236, doi:10.1073/pnas.1421816112, 2015.

5   Oguri, K., Kawamura, K., Sakaguchi, A., Toyofuku, T., Kasaya, T., Murayama, M., Fujikura, K., Glud, R. N. and Kitazato, H.: Hadal disturbance in the Japan Trench induced by the 2011 Tohoku–Oki Earthquake, Sci Rep, 3, 1915, doi:10.1038/srep01915, 2013.

Okumura, T., Kawagucci, S., Saito, Y., Matsui, Y., Takai, K. and Imachi, H.: Hydrogen and carbon isotope systematics in hydrogenotrophic methanogenesis under H_2-limited and H_2-enriched conditions: implications for the origin of methane

10   and its isotopic diagnosis, Progress in Earth and Planetary Science, 3, 14, doi:10.1186/s40645-016-0088-3, 2016a.

Okumura, T., Ohara, Y., Stern, R. J., Yamanaka, T., Onishi, Y., Watanabe, H. K., Chen, C., Bloomer, S. H., Pujana, I., Sakai, S., Ishii, T. and Takai, K.: Brucite chimney formation and carbonate alteration at the Shinkai Seep Field, a serpentinite-hosted vent system in the southern Mariana forearc, Geochem. Geophys. Geosyst., 17, doi:10.1002/2016GC006449, 2016b.

15   Popp, B. N., Westley, M. B., Toyoda, S., Miwa, T., Dore, J. E., Yoshida, N., Rust, T. M., Sansone, F. J., Russ, M. E., Ostrom, N. E. and Ostrom, P. H.: Nitrogen and oxygen isotopomeric constraints on the origins and sea-to-air flux of N_2O in the oligotrophic subtropical North Pacific gyre, Global Biogeochem. Cycles, 16(4), 1064, doi:10.1029/2001GB001806, 2002.

Reeburgh, W.S.: Oceanic methane biogeochemistry, Chem. Rev., 107, 486-513, 2007.

20   Resing, J. A., Sedwick, P. N., German, C. R., Jenkins, W. J., Moffett, J. W., Sohst, B. M. and Tagliabue, A.: Basin-scale transport of hydrothermal dissolved metals across the South Pacific Ocean, Nature, 523(7559), 200–203, doi:10.1016/S0016-7037(96)00304-3, 2015.

Shiozaki, T., Ijichi, M., Isobe, K., Hashihama, F., Nakamura, K.-I., Ehama, M., Hayashizaki, K.-I., Takahashi, K., Hamasaki, K. and Furuya, K.: Nitrification and its influence on biogeochemical cycles from the equatorial Pacific to the Arctic

25   Ocean, ISME J., 10(9), 2184–2197, doi:10.1038/ismej.2016.18, 2016.

Siedler, G., Church, J., and Gould, J. (eds.): Ocean Circulation and Climate: Observing and Modelling the Global Ocean, Academic Press, London, UK, 2001.

Son, J., Pak, S.-J., Kim, J., Baker, E. T., You, O.-R., Son, S.-K. and Moon, J.-W.: Tectonic and magmatic control of hydrothermal activity along the slow-spreading Central Indian Ridge, 8°S-17°S, Geochem. Geophys. Geosyst., 15(5),

30   2011–2020, doi:10.1002/ggge.20243, 2014.

Taira, K.: Super-deep CTD Measurements in the Izu-Ogasawara Trench and a Comparison of Geostrophic Shears with Direct Measurements, Journal of Oceanography, 62, 753–758, 2006.

Taira, K., Yanagimoto, D., and Kitagawa, S.: Deep CTD Casts in the Challenger Deep, Mariana Trench, Journal of Oceanography, 61, 447–454, 2005.

Toyoda, S., Yoshida, N., Miwa, T., Matsui, Y., Yamagishi, H., Tsunogai, U., Nojiri, Y. and Tsurushima, N.: Production mechanism and global budget of N_2O inferred from its isotopomers in the western North Pacific, Geophys. Res. Lett., 29(3), 2002.

Toyoda, S., Yoshida, N. and Koba, K.: Isotopocule analysis of biologically produced nitrous oxide in various environments, Mass Spec. Rev., 36, 135–160, doi:10.1016/j.jinorgbio.2004.09.024, 2017.

Tsunogai, U., Ishibashi, J.-I., Wakita, H., Gamo, T., Watanabe, K., Kajimura, T., Kanayama, S. and Sakai, H.: Peculiar features of Suiyo Seamount hydrothermal fluids, Izu-Bonin Arc: Differences from subaerial volcanism, Earth and Planetary Science Letters, 126, 289–301, 1994.

Tsunogai, U., Ishibashi, J.-I., Wakita, H., Gamo, T., Masuzawa, T., Nakatsuka, T., Nojiri, Y. and Nakamura, T.: Fresh water seepage and pore water recycling on the seafloor: Sagami Trough subduction zone, Japan, Earth and Planetary Science Letters, 138, 157–168, 1996.

Tsunogai, U., Ishibashi, J.-I., Wakita, H. and Gamo, T.: Methane-rich plumes in the Suruga Trough (Japan) and their carbon isotopic characterization, Earth and Planetary Science Letters, 160, 97–105, 1998.

Tsunogai, U., Yoshida, N., Ishibashi, J.-I. and Gamo, T.: Carbon isotopic distribution of methane in deep-sea hydrothermal plume, Myojin Knoll Caldera, Izu-Bonin arc: Implications for microbial methane oxidation in the oceans and applications to heat flux estimation, Geochimica et Cosmochimica Acta, 64, 2439–2452, 2000.

Uchida, H., Nakano, T., Tamba, J., Widiatmo, J.V., Yamazawa, K., Ozawa, S. and Kawano, T.: Deep ocean temperature measurement with an uncertainty of 0.7 mK, J. Atmos. Oceanic Technol., 32, 2199–2210, 2015.

Wakita, M., Honda, M. C., Matsumoto, K., Fujiki, T., Kawakami, H., Yasunaka, S., Sasai, Y., Sukigara, C., Uchimiya, M., Kitamura, M., Kobari, T., Mino, Y., Nagano, A., Watanabe, S. and Saino, T.: Biological organic carbon export estimated from the annual carbon budget observed in the surface waters of the western subarctic and subtropical North Pacific Ocean from 2004 to 2013, Journal of Oceanography, 72(5), 665–685, doi:10.1007/s10872-016-0379-8, 2016.

Walting, L., Guinotte, J., Clark, M.R., Smith, C.R.: A proposed biogeography of the deep ocean floor, Progress in Oceanography, 111, 91-112, 2013.

Wenzhöfer, F., Oguri, K., Middelboe, M., Turnewitsch, R., Toyofuku, T., Kitazato, H. and Glud, R. N.: Benthic carbon mineralization in hadal trenches: Assessment by in situ O_2 microprofile measurements, Deep-Sea Research Part I, 116(c), 276–286, doi:10.1016/j.dsr.2016.08.013, 2016.

Wijffels, S.E., Hall, M.M., Joyce, T., Torres, D.J., Hacker, P. and Firing, E.: Multiple deep gyres of the western North Pacific: A WOCE section along 149ºE, J. Geophys., Res., 103(C6), 12,985−13,009, 1998.

Zhang, J.-Z., and Ortner. P. B.: Effect of thawing condition on the recovery of reactive silicic acid from frozen natural water samples. Water Res., 32, 2553-2555, 1998.

Tables and Figures

Table 1: Summary of stations.

Cruise	Station	YYYYMMDD	Lat degree	Lat minute	Lon degree	Lon minute	Depth (m)	**Relative location
KM16-02	31N01	20160505	31	18.2	141	46.7	5801	WW
KM16-02	31N03	20160506	31	20.0	142	14.5	9382	A
KM16-02	31N02	20160507	31	18.3	142	0.3	7093	W
KM16-02	31N04	20160507	31	19.1	142	38.9	6928	E
KM16-02	31N05	20160507	31	19.8	143	0.1	6162	EE
KS-16-8	30N01	20160708	30	0.0	142	36.3	9190	A
KS-16-8	32N01	20160711	32	9.0	142	0.0	7931	W
KS-16-8	32N02 (KEO)	20160706	32	21.6	144	24.2	5737	EE
KM16-08	34N03	20160913	34	57.6	142	33.5	5837	E
KM16-08	34N02	20160914	34	0.1	141	57.2	9224	A
KM17-01	29N02	20170106	29	17.6	143	30.8	6062	E
KM17-01	29N01	20170107	20	8.9	142	48.9	9820	A
KM17-01	26N01	20170108	26	10.3	143	15.2	3306	(A)
KM17-01	27N01	20170108	27	30.1	143	19.1	8949	A
KM17-01	24N01	20170109	24	16.4	143	38.3	8798	A
KM17-01	24N02	20170109	24	15.5	144	15.0	4898	E
KH-84-3	AN1*	19840823-30	29	5.0	142	51.0	9768	A
KH-94-3	LM2*	19941004-06	29	4.8	142	50.0	9738	A
*Gamo and Shitashima 2018								
**Relative locations from trench axis. WW: far west, W: west, A: Axis, E: east, EE: far east								

Table 2: Summary of analyses.

		DO	Nitrate	$\delta^{15}N_{N+N}$	$\delta^{18}O_{N+N}$	PO$_4$	SiO$_2$	N$_2$O	$\delta^{15}N_{N2O}$	$\delta^{18}O_{N2O}$	TOC	$\Delta^{14}C$
		umol/kg	umol/kg	permil	permil	umol/kg	umol/kg	nM	permil	permil	uM	permil
Izu-Ogasawara (this study)	AVG	164.0	35.2	5.10	2.23	2.46	145.6	17.7	8.82	51.56	37.9	-206.6
	STD	0.27	0.41	0.15	0.11	0.06	0.2	1.3	0.22	0.26	1.1	4.4
	n	47	47	25	25	23*	11*	47	47	47	45	40
Izu-Ogasawara (G&S2018)	AVG	165.7	35.1	NA	NA	2.39	~142	NA	NA	NA	NA	NA
	STD	0.7	0.3			0.04						
Mariana (this study)	AVG	171.7	34.7	5.13	2.24	NA	NA	17.1	8.70	51.11	37.6	-197.0
	STD	0.04	0.05	0.08	0.05			0.8	0.10	0.24	0.6	3.9
	n	10	10	7	7			10	10	10	10	10
	*Data available only from KM16-08 cruise											

Figure 1: Seafloor topography of (a) western North Pacific and (b-g) cross section of inner trench. Horizontal red lines in panel (a) represent the sections shown in panels (b-g). Vertical dash lines in panels (b-g) represent CTD-CMS stations (see Table 1).

Figure 2: Vertical profiles of measured parameters. Symbol shapes and colours are classified by locations relative to the axis and latitude, respectively (see Table 1). Horizontal dash lines indicate the abyssal-hadal boundary. Bold horizontal lines shown at the bottom of each panel represent one-sigma analytical errors whereas not shown when the errors are smaller than symbol size.

Figure 3: Vertical profiles of (a) $\delta^{15}N_{N+N}$ increase of cultivated batches from control batch after ^{15}N-spiked incubation and (b) nitrification activity calculated based on the $\delta^{15}N_{N+N}$ differences. Since the $\delta^{15}N_{N+N}$ increase three times greater than analytical uncertainty (>0.6‰) is regarded as significant, symbols fallen into grey shadow in panel (a) represent insignificant activity. Symbol colours of red, blue, and green respectively represent 15N-labeled substrates of ammonium, urea, and glutamine. Horizontal axes are presented in logarithmic scale.

Figure 4: A DO-$\Delta^{14}C$ plot for deep seawater (>4,000 dbar). Symbols with colour are same with those in Figure 2. Filled black circles and a diagonal line respectively represent a dataset from WOCE P01-P03 stations and its fitting line.

Figure 5: Spatial distribution of $\delta^{13}C_{CH4}$ values. Symbols are classified by colour according to relative locations from trench axis. Long horizontal bars indicate the boundary between Izu-Ogasawara and Mariana trenches, Ogasawara Plateau.

Figure 6: A plot between CH_4 concentration and $\delta^{13}C_{CH4}$. Symbols with colour are same with those in Figure 2. Open and filled stars respectively represent endmember values assumed for background seawater and inner-trench CH_4 source. Broken curves represent theoretical isotope behaviours from the local CH_4 source when kinetic isotope effects on microbial methanotrophy (ε) are 5 and 20. A broken-dot curve represents a bimodal mixing between two endmembers.
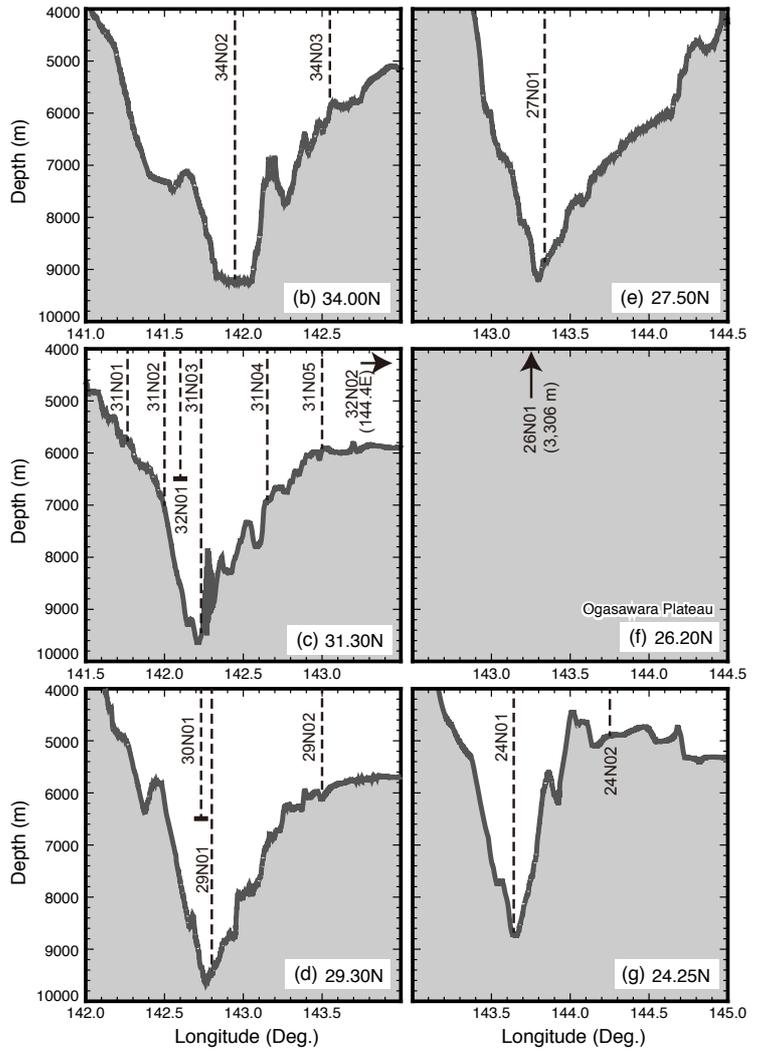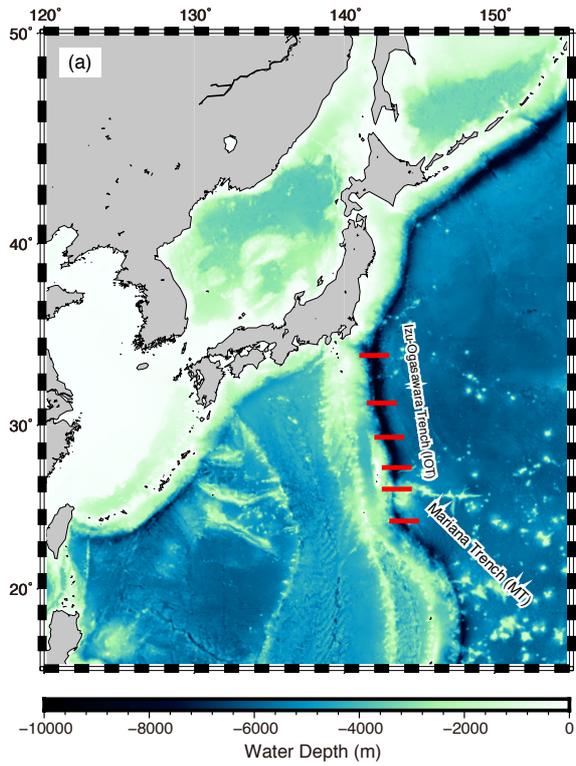
Figure 1 (Kawagucci et al.)
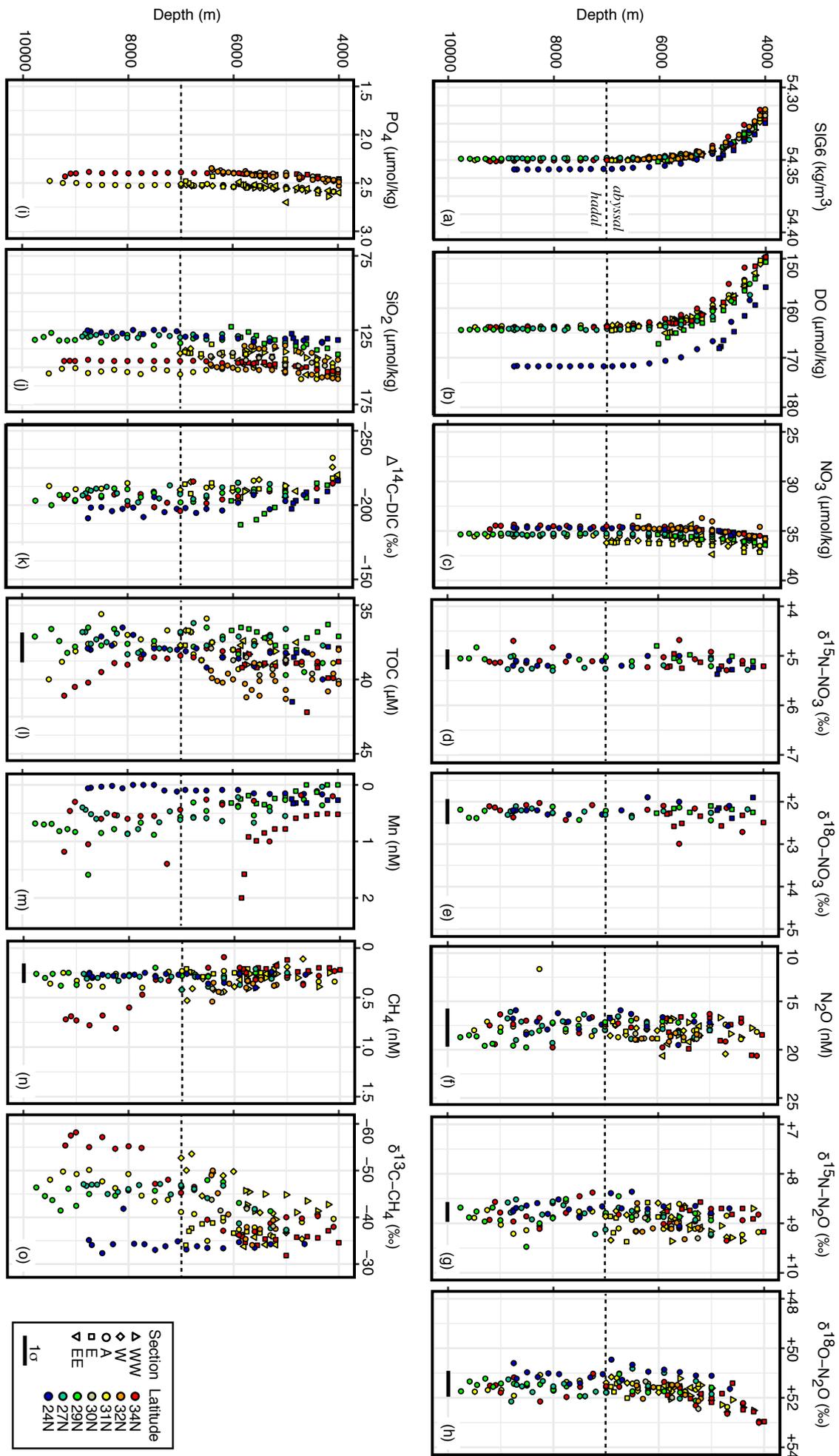
Figure 2 (Kawagucci et al.)
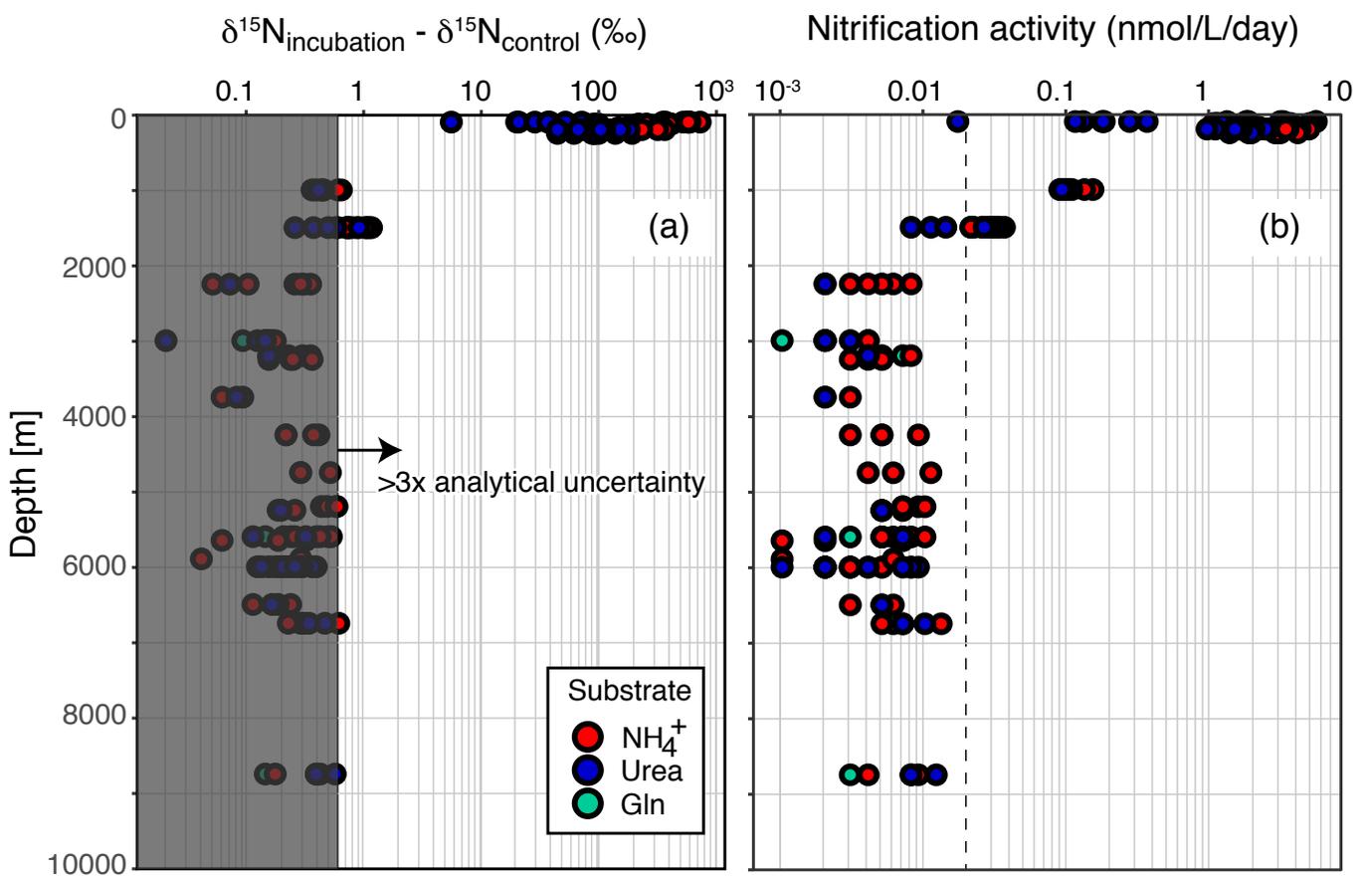
Figure 3 (Kawagucci et al.)
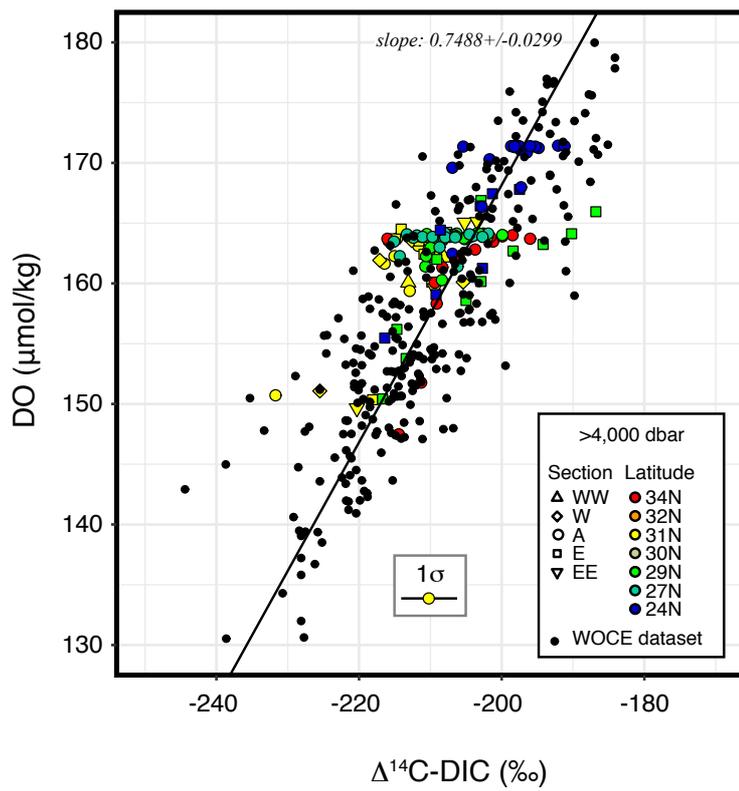
Figure 4 (Kawagucci et al.)
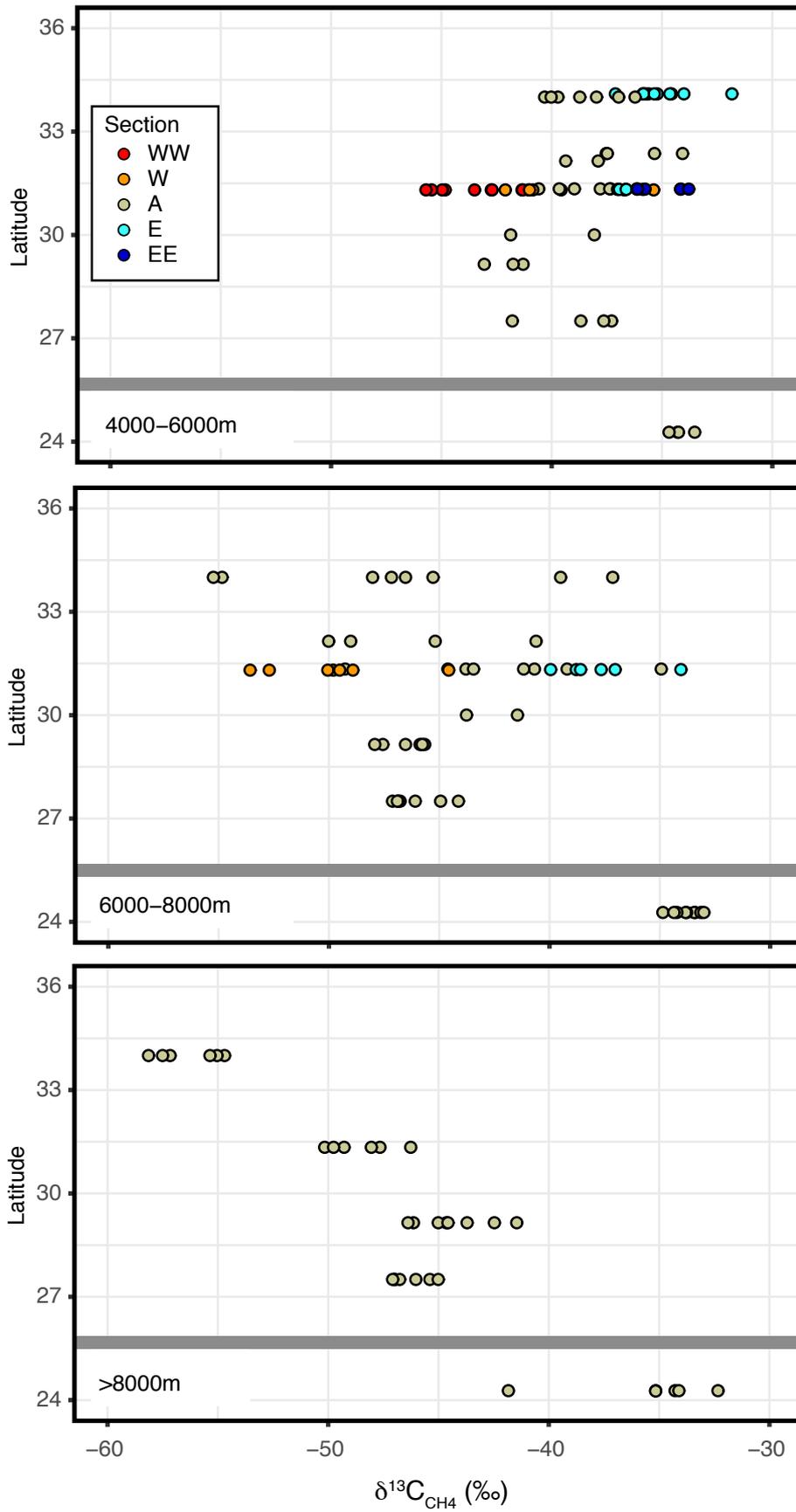
Figure 5 (Kawagucci et al.)

Figure 6 (Kawagucci et al.)